

Large magnetoresistance in LaBi: origin of field-induced resistivity upturn and plateau in compensated semimetals

Shanshan Sun^{1,†}, Qi Wang^{1,†}, Peng-Jie Guo^{1,†}, Kai Liu¹, and Hechang Lei^{1,*}

¹*Department of Physics and Beijing Key Laboratory of Opto-electronic Functional Materials & Micro-nano Devices, Renmin University of China, Beijing 100872, China*

(Dated: December 3, 2024)

The discovery of non-magnetic extreme magnetoresistance (XMR) materials has induced great interests because of their great importance to understanding the response of carrier to electric and magnetic fields and significant application values. Among XMR materials, the LaSb shows XMR and field-induced exotic behaviors but it seems to lack the essentials for these properties. Here, we study the magnetotransport properties and electronic structure of LaBi, isostructural to LaSb. LaBi exhibits large MR as in LaSb, which can be ascribed to the (nearly) compensated electron and hole with rather high mobilities. More importantly, our analysis suggests that the XMR, field-induced resistivity upturn, and plateau observed in LaSb and LaBi can be well explained by the two-band model with the compensation situation. We present the critical conditions leading to these field-induced properties. It will contribute to understanding the XMR phenomenon and exploring novel XMR materials.

PACS numbers: 72.15.-v, 72.15.Gd, 71.30.+h, 71.20.Eh

Magnetoresistance (MR) that electronic resistance changes with magnetic field not only is one of the most important topics in the area of condensed matter physics but also induces long-term research interests for practical applications, such as magnetic field sensors, read heads of hard drives, random access memories [1]. In general, the large MR is emergent in magnetic materials, such as giant MR (GMR, $MR \sim 10^2$ %) in metallic thin films and colossal MR (CMR, $MR \sim 10^4$ %) in Cr-based chalcogenide spinels as well as Mn-based perovskites [2–4]. In the past several years, a series of non-magnetic metals with extreme MR (XMR) has been discovered, such as TmPn (Tm = Nb and Ta, Pn = P and As) [5–7], Cd₃As₂ [8], and WTe₂ [9]. These discoveries greatly challenge the traditional understanding that the non-magnetic metals usually have a small MR of only about a few percent. These novel XMR materials exhibit some common features, such as the extremely high mobilities μ , usually $\mu > 1 \times 10^4$ cm² V⁻¹ s⁻¹, and comparable carrier concentrations of electron and hole in many of them [5–9]. Based on these features, several mechanisms have been proposed to explain the origin of XMR in these materials, including topological protection from backscattering mechanism in Dirac and Weyl semimetals (SMs) [7, 8], and electron-hole compensation mechanism [9].

Very recently, the XMR material is extend to the rare-earth-based material LaSb with simple rock-salt structure [10]. It shows XMR at 2 K and 9 T (0.9×10^6 %). Moreover, metallic LaSb exhibits the field-induced upturn behavior in resistivity curve appearing at low temperature, followed by a resistivity plateau [10]. Similar phenomena are also observed in several systems, such as NbP and WTe₂ [6, 9]. However, the prerequisites for XMR and related field-induced properties seem absent in LaSb, such as the inversion symmetry broken as in Weyl SMs, linear dispersion of band structure near

Fermi energy level E_F as in Dirac SMs, and perfect electron-hole compensation satisfying the resonance situation as in WTe₂. Thus, LaSb provides an novel platform for understanding the field-induced properties in SMs. On the other hand, a recent theoretical study predicted that lanthanum monopnictides (LaPn) are three-dimensional (3D) topological insulators (TIs) or topological SMs (TSMs) [11].

In order to explore more XMR materials and possible TIs/TSMs in this family and understand field-induced properties in LaSb as well as other XMR materials, here, we report the detailed study on magnetotransport properties and electronic structure of LaBi single crystals, isostructural to LaSb. We find LaBi exhibits similar XMR and field-induced behaviors as in LaSb. Based on the classical two-band model, we proposed a theoretical explanation that can well resolve the origin of XMR and field-induced phenomena not only in LaPn, but also in other XMR materials.

Single crystals of LaBi were grown by In flux. The elements were put into alumina crucible and sealed in quartz ampoule under partial argon atmosphere. The sealed quartz ampoule was heated to and soaked at 1323 K, then slowly cooled down to 1123 K. Finally, the ampoule was decanted with a centrifuge. X-ray diffraction (XRD) of a single crystal were performed using a Bruker D8 X-ray machine. Resistivity were measured using four-probe configuration in a Quantum Design PPMS-14T. The first-principles electronic structure calculations were implemented with the projector augmented wave method [12] as implemented in the VASP package [13]. For the exchange-correlation potential, the generalized gradient approximation of Perdew-Burke-Ernzerhof type [14] was used. The kinetic energy cutoff of the plane wave basis was set to be 300 eV. For the Brillouin zone sampling, a $10 \times 10 \times 10$ k-point mesh was employed. Both cell pa-

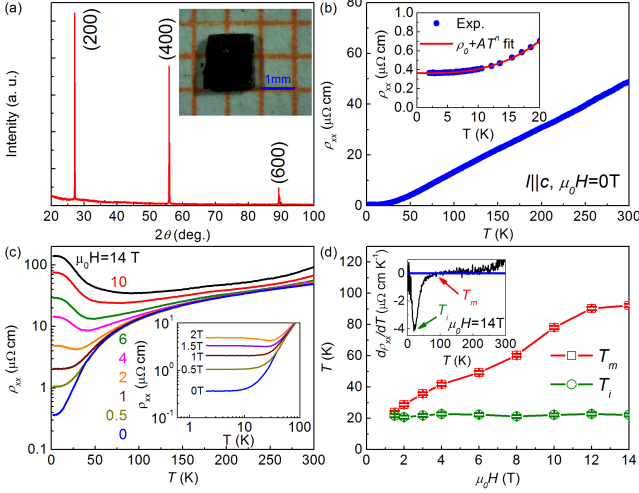


FIG. 1. (a) XRD of a LaBi single crystal at 300 K. Inset: photo of typical LaBi single crystal. (b) Temperature dependence of $\rho_{xx}(T, 0)$ for $I \parallel c$. Insets: enlarged parts of $\rho_{xx}(T, 0)$ below 20 K. The solid line is the fit using the formula $\rho_{xx}(T, 0) = \rho_0 + AT^n$. (c) Temperature dependence of $\rho_{xx}(T, \mu_0 H)$ at various fields. Inset: enlarged parts of $\rho_{xx}(T, \mu_0 H)$ at low-temperature region under low fields. (d) Field dependence of T_m and T_i , corresponding to the sign change and the minimum in the $d\rho_{xx}(T, \mu_0 H)/dT$ curves, respectively. Inset: $d\rho_{xx}(T, \mu_0 H)/dT$ vs. T at 14 T. The positions of T_m and T_i are marked by arrows.

rameters and internal atomic positions were allowed to relax until all forces on atoms were smaller than 0.01 eV/Å. The spin-orbital-coupling effect was included in the calculations of electronic properties. The maximally localized Wannier functions [15, 16] was used to calculate the Fermi surfaces (FSs), which were prepared with the XCRYSDEN program [17].

The XRD pattern of a LaBi single crystal indicates that the surface of crystal is the (1 0 0) plane (Fig. 1(a)). The cubic-shape LaBi crystals (inset of Fig. 1(a)) is consistent with the single crystal XRD pattern and its crystallographic symmetry. As shown in Fig. 1(b), the zero-field resistivity $\rho_{xx}(T, 0)$ of LaBi single crystal exhibits metallic behavior, similar to that in LaSb [10]. The residual resistance ratio [RRR $\equiv R(300 \text{ K})/R(2 \text{ K}) = 137$] indicates the high quality of sample. The linear temperature dependence of $\rho_{xx}(T, 0)$ at high temperatures suggests the electron-phonon (e - ph) scattering is the dominant scattering mechanism. In contrast, the $\rho_{xx}(T, 0)$ at low-temperature region ($2 \text{ K} \leq T \leq 20 \text{ K}$) can be well fitted by using the formula $\rho_{xx}(T, 0) = \rho_0 + AT^n$ with $\rho_0 = 0.3623(5) \mu\Omega \text{ cm}$ and $n = 2.96(3)$ (inset of Fig. 1(b)). The value of ρ_0 is larger than that in LaSb ($\rho_0 = 0.08 \mu\Omega \text{ cm}$) but the n is smaller ($n = 4$ for LaSb) [10]. The values of n for both systems distinctly different from $n = 2$ when e - e scattering is dominant, such as in WTe₂ [18]. These values are also smaller than $n = 5$ for the conventional e - ph scattering process according

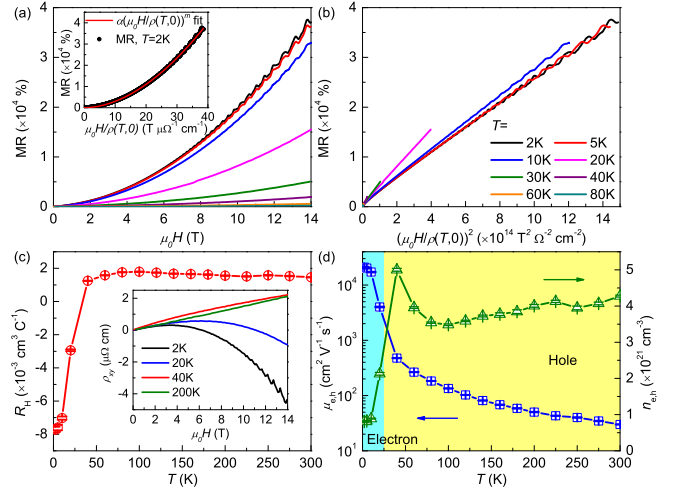


FIG. 2. (a) MR up to 14 T at $T \leq 80 \text{ K}$. The color code is same as in (b). Inset: MR at 2 K. The solid line is the fit using $\alpha[\mu_0 H/\rho_{xx}(T, 0)]^m$. (b) MR vs. $[\mu_0 H/\rho_{xx}(T, 0)]^2$ at $T \leq 80 \text{ K}$. (c) Temperature dependence of R_H determined from the slope of $\rho_{xy}(T, \mu_0 H)$ between 10 - 14 T. Inset plots the $\rho_{xy}(T, \mu_0 H)$ at several temperatures. (d) Temperature dependence of the $n_{e,h}$ and $\mu_{e,h}$ derived using the single-carrier model. The temperature regions where electrons and holes act as the main charge carriers are marked with light cyan and yellow shadings, respectively.

to the Bloch-Grüneisen theory [19]. It suggests that the interband s - d e - ph scattering, rather than the intraband s - s e - ph scattering should be dominant at low temperature [19]. Similar behavior has been observed in yttrium metal as well as in other transition metal carbide [20, 21].

Fig. 1(c) shows the $\rho_{xx}(T, \mu_0 H)$ at various fields up to 14 T. When the field is low, the $\rho_{xx}(T, \mu_0 H)$ still exhibits metallic behavior in the whole temperature region, similar to the $\rho_{xx}(T, 0)$. Once the field is beyond the critical field $\mu_0 H_c$ ($\sim 1.5 \text{ T}$) (inset of Fig. 1(c)), the $\rho_{xx}(T, \mu_0 H)$ curves show a minimum at field-dependent "turn-on" temperatures $T_m(\mu_0 H)$, i.e., the $\rho_{xx}(T, \mu_0 H)$ increases significantly with decreasing temperature. This behavior has been observed not only in LaSb but also in other XMR materials, such as WTe₂ and NbP [6, 9, 10]. Correspondingly, when $\mu_0 H > \mu_0 H_c$, the $d\rho_{xx}(T, \mu_0 H)/dT$ is positive at $T > T_m$ and changes the sign at $T < T_m$ (inset of Fig. 1(d)). When the field increases, the T_m shifts to higher temperature, but another characteristic temperature T_i related to the inflection point of $\rho_{xx}(T, \mu_0 H)$ seems insensitive to the field (Fig. 1(d)). Both characteristic temperatures merge together when $\mu_0 H \sim \mu_0 H_c$. Moreover, there is a plateau in $\rho_{xx}(T, \mu_0 H)$ curves following the upturn behavior at low temperatures and high fields. Similar behaviors have been observed in LaSb [10].

LaBi exhibits rather large MR ($= (\rho_{xx}(T, \mu_0 H) - \rho_{xx}(T, 0))/\rho_{xx}(T, 0) = \Delta\rho_{xx}(T, \mu_0 H)/\rho_{xx}(T, 0)$) at low temperature and the MR at 2 K is $3.8 \times 10^4 \%$ under 14 T (Fig. 2(a)). Although the MR at 9 T ($\sim 1.6 \times 10^4$

%) is one order of magnitude smaller than that in LaSb, it is still comparable with the MRs in other XMR materials [5, 8, 10]. The MR of LaBi does not saturate up to 14 T and when the field is larger than about 5 T, the Shubnikov-de Haas (SdH) quantum oscillations (QOs) appears at low temperature (Fig. 2(a)). The MR decreases gradually below 10 K, but drops quickly at higher temperatures. According to the Kohler's rule [18, 19], $MR = \alpha(\mu_0 H / \rho_{xx}(T, 0))^m$, if the carrier concentration of sample is weakly temperature dependent, the MR measured at various temperatures can be scaled into a single curve. But the scaled MR curves do not fall into one curve for LaBi (Fig. 2(b)), obviously deviating from the Kohler's rule. This violation strongly suggests that the carrier concentrations and/or the mobility ratio of hole to electron change significantly with temperature [18, 22]. The fit of MR curve at 2 K gives $\alpha = 0.411(4)$ ($\mu\Omega \text{ cm/T}$)^{1.866} and $m = 1.866(2)$ (inset of Fig. 2(a)), close to the typically quadratic field dependence of the MR in the multiband metals.

Hall resistivity $\rho_{xy}(T, \mu_0 H)$ of LaBi (inset of Fig. 2(c)) is positive at high temperature with linear field dependence, suggesting the hole is dominant. With lowering temperature, the $\rho_{xy}(T, \mu_0 H)$ exhibits nonlinear behavior and becomes negative at high field. It implies that at low temperatures the carrier concentration of electron n_e is slightly larger than that of hole n_h but the mobility has opposite relation, e.g., $\mu_e < \mu_h$. Moreover, the QOs are clearly seen at 2 K, consistent with the MR results. Using the slope of $\rho_{xy}(T, \mu_0 H)$, at high field region (10 - 14 T), the calculated high-field Hall coefficient $R_H(T)$ is positive and weakly temperature dependent above 40 K and changes dramatically below 40 K with the sign reversing (Fig. 2(c)). According to the single-carrier model, $n_{e,h}(T) = 1/(eR_H(T))$ and $\mu_{e,h}(T) = R_H(T)/\rho_{xx}(T, 0)$, the $n_{e,h}(T)$ and $\mu_{e,h}(T)$ can be estimated qualitatively (Fig. 2(d)). The $n_{e,h}(T)$ exhibits strong temperature dependence especially below 40 K, leading to the violation of Kohler's rule (Fig. 2(b)). The estimated $n_{e,h}(2 \text{ K})$ is $8.1(2) \times 10^{20} \text{ cm}^{-3}$. Such small $n_{e,h}$ with two types of carriers confirms the semimetallicity of LaBi. In contrast, the $\mu_{e,h}(T)$ monotonically increases with decreasing temperature with a larger slope below 40 K and the $\mu_{e,h}(2 \text{ K})$ is rather high ($2.10(4) \times 10^4 \text{ cm}^2 \text{ V}^{-1} \text{ s}^{-1}$). The $n_{e,h}$ is larger but the $\mu_{e,h}$ is about one order magnitude smaller than those in LaSb at 2 K [10].

The QOs as a function of $1/(\mu_0 H)$ at low temperatures are shown in Fig. 3(a). The amplitudes of QOs decrease with increasing temperature or decreasing field. The fast Fourier transform (FFT) spectra of the QOs reveals two principal frequencies $F_\alpha = 276 \text{ T}$ with its second harmonic frequency $F_{2\alpha} = 555 \text{ T}$ and $F_\beta = 610.5 \text{ T}$ (Fig. 3(b)). All of these frequencies are higher than those in LaSb [10], indicating LaBi has larger FSs than LaSb, agreeing with the results of Hall measurement [10]. According to the Onsager relation $F = (\hbar/2\pi e)A_F$, where

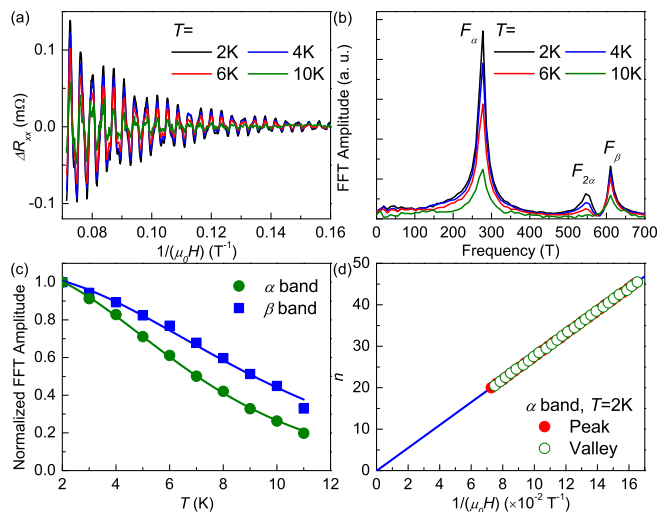


FIG. 3. (a) SdH QOs $\Delta R_{xx} = R_{xx} - \langle R_{xx} \rangle$ as a function of $1/(\mu_0 H)$ at various temperatures. (b) FFT spectra of the QOs at various temperatures. (c) The temperature dependence of FFT amplitudes of α and β peaks, normalized by their 2 K values. The solid lines are the fits using the LK formula, giving the effective masses. (d) The Landau level indices n as a function of $1/(\mu_0 H)$ for the α band. The solid and empty symbols correspond to the positions of peaks and valleys in ΔR_{xx} curve at 2 K, respectively. The solid line represents the linear fit of data.

A_F is the extremal cross section of FS. The determined A_F is 0.027 and 0.058 \AA^{-2} for α and β bands, respectively, consistent with previous results [23]. These A_F s are very small, taking only ~ 2.9 and 6.4% of the whole area of Brillouin zone in the $k_x - k_y$ plane providing the lattice parameter $a = 6.58 \text{ \AA}$. Because the β band is almost spherical [23], the estimated carrier concentration for β band n_h^β is $0.85 \times 10^{20} \text{ cm}^{-3}$. The effective mass m^* can be extracted from the temperature dependence of the amplitude of FFT peak using the Lifshitz-Kosevich (LK) formula [24]. The m^* of α and β band is $0.217(1)$ and $0.164(3) m_e$, respectively, where m_e is the bare electron mass (Fig. 3(c)). The fitted Dingle temperature from the decaying amplitude of QOs with field at 2 K [24] gives $T_D^\alpha = 9(1) \text{ K}$ for the α band, corresponding to the quantum lifetime $\tau_Q^\alpha = \frac{\hbar}{2\pi k_B T_D^\alpha} = 1.2(2) \times 10^{-13} \text{ s}$. The Landau Level (LL) index n is related to the QO frequency F by the Lifshitz-Onsager quantization rule $F/(\mu_0 H) = n + 1/2 - \phi_B/2\pi + \delta$, where ϕ_B is the Berry phase, δ is a phase shift determined by the dimensionality ($\delta = \pm 1/8$ for the 3D system) [24–26]. The peaks and valleys of the ΔR_{xx} at 2 K are assigned as integer (n) and half integer ($n + 1/2$) LL indices, respectively. Linear fit of n vs. $1/(\mu_0 H)$ yields $F = 275.9(4) \text{ T}$ and $1/2 - \phi_B/2\pi + \delta = -0.05(5)$ (Fig. 3(d)), indicating a possible non-trivial Berry's phase for the α band. It needs to be further confirmed by the measurement at higher field in order to reach the quantum limit.

Similar to LaSb [10, 11], theoretical calculation indi-

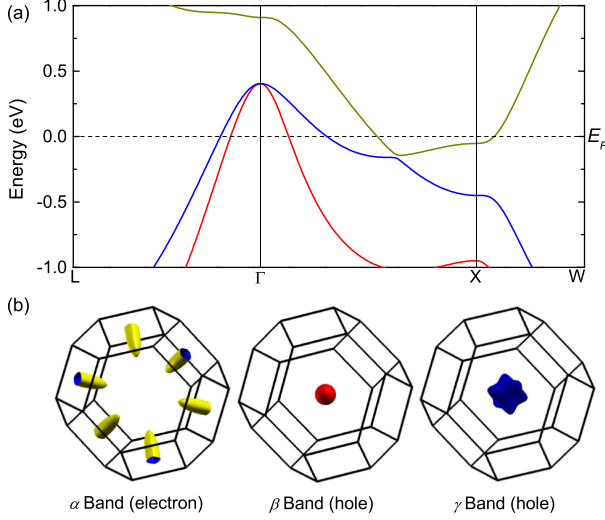


FIG. 4. (a) Band structure and (b) FSs of LaBi. The dashed line denotes the position of E_F . There are three FSs at E_F , including two hole-type FSs around Γ point and one electron-type FS around X point.

cates that there are three bands crossing E_F in LaBi (Fig. 4(a)), consistent with QOs results [23]. The electron-type band (α band) is located at X point with the ellipsoidal FS with longest principle axis along $\Gamma - X$ line; Two hole-type bands (β and γ bands) are centered at Γ point. One has a nearly spherical FS and another one has a FS stretched in the $\langle 1\ 0\ 0 \rangle$ directions (Fig. 4(b)). The calculated $n_{e,h}$ are 3.52 , 0.72 , and $2.88 \times 10^{20} \text{ cm}^{-3}$ for the α , β , and γ bands, strongly indicating that LaBi is a nearly compensated SM ($\lambda = n_e/n_h = 0.98$).

Because LaSb and LaBi seem nearly compensated SMs, similar to WTe_2 , we develop the model proposed to explain the magnetotransport properties of WTe_2 [18] to analysis the common features in (nearly) compensated SMs. According to the two-band model [18, 19], the MR can be expressed

$$MR = \frac{n_e \mu_e n_h \mu_h (\mu_e + \mu_h)^2 (\mu_0 H)^2}{(n_e \mu_e + n_h \mu_h)^2 + (n_e - n_h)^2 (\mu_e \mu_h)^2 (\mu_0 H)^2} \quad (1)$$

For the compensated SMs ($n_e = n_h = n_c$), we have $MR = \mu_e \mu_h (\mu_0 H)^2$. Thus, the large MR is directly related to the high mobilities of materials. If assuming $\rho_{xx}(T, 0) = \rho_0 + AT^n$, we get

$$\rho_{xx}(T, \mu_0 H) = \rho_0 + AT^n + \alpha (\mu_0 H)^2 / (\rho_0 + AT^n) \quad (2)$$

where $\alpha = \kappa [n_c e (1 + \kappa)]^{-2}$ and $\kappa = \mu_e / \mu_h$ [18]. Therefore, we will return to the Kohler's rule with $m = 2$. More importantly, according to eq. (2), there is a minimum in $\rho_{xx}(T, \mu_0 H)$ curve when $\mu_0 H > \mu_0 H_c (= \rho_0 / \alpha^{1/2})$ [18], i.e., field-induced resistivity upturn. The simulated $\rho_{xx}(T, \mu_0 H)$ curves with $\mu_0 H_c = 1$ clearly reflect

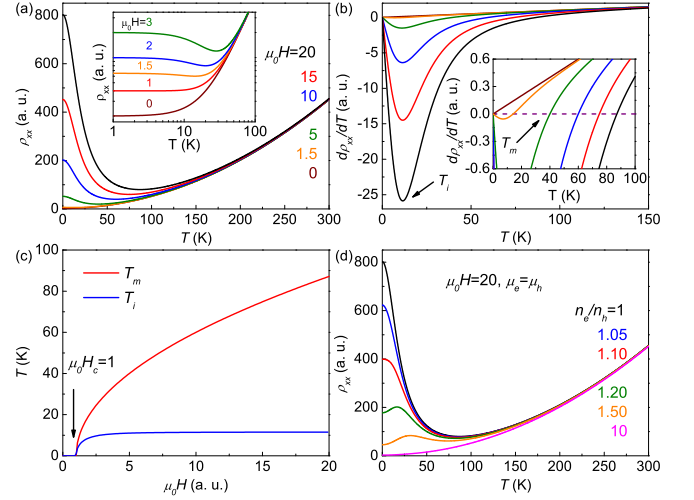


FIG. 5. Simulation of longitudinal resistivity using eq. (2) with $\rho_0 = 2$, $A = 5 \times 10^{-3}$, $\alpha = 4$, and $n = 2$. (a) Temperature dependence of simulated $\rho_{xx}(T, \mu_0 H)$ at various fields with $\mu_0 H_c = 1$. Inset: simulated $\rho_{xx}(T, \mu_0 H)$ vs. T when the fields are near $\mu_0 H_c$. (b) Corresponding $d\rho_{xx}(T, \mu_0 H)/dT$ as a function of T at various fields. Inset displays the changes of T_m with field. (c) Field dependence of derived T_m and T_i . (d) $\rho_{xx}(T, \mu_0 H)$ vs. T at various n_e/n_h with $\mu_0 H = 20$.

this behavior and well reproduce the experimental results (Fig. 5(a)). Firstly, because the ρ_0 and n_c in LaBi are larger than those in LaSb [10, 23], the $\mu_0 H_c$ (~ 1.5 T) for LaBi is large than that in LaSb ($\mu_0 H_c = 0.4(1)$ T) [10]. Secondly, the $\rho_{xx}(0, \mu_0 H)$ is not infinity but $\rho_0 + \alpha (\mu_0 H)^2 / \rho_0$, i.e., there is a resistivity plateau at low temperature with the absolute value increasing at higher field. Thirdly, the simulated T_m and T_i well reflect the features observed in LaSb [10] and LaBi (Fig. 5(b) and (c)). The T_m is proportional to $(\mu_0 H - \mu_0 H_c)^{1/n}$ (here, $n = 2$) and the T_i saturates quickly when field is large. Noted that the $T_i(\mu_0 H_c)$ becomes zero but this trend is not observed experimentally, possibly because the initial slope of $T_i(\mu_0 H)$ is very large and the $\rho_{xx}(T, \mu_0 H)$ is too flat to extract accurate T_i when $\mu_0 H$ is close to $\mu_0 H_c$. Finally, we examine the influence of the uncompensation between electron and hole on the field-induced resistivity upturn. If assuming $\mu_e = \mu_h$, we get

$$\rho_{xx}(T, \mu_0 H) = \rho_0 + AT^n + \frac{4\lambda(\rho_0 + AT^n)(\mu_0 H)^2}{\beta^2(\rho_0 + AT^n)^2(\lambda + 1)^4 + (\lambda - 1)^2(\mu_0 H)^2} \quad (3)$$

where $\beta = \frac{1}{2\sqrt{\alpha}}$. When λ increases, although the $\rho_{xx}(0, \mu_0 H)$ decreases gradually, there is still a remarkable resistivity upturn with a plateau even extending to the higher temperature (Fig. 5(d)). It indicates that the field-induced resistivity upturn is robust to the imbalance between n_e and n_h . Surprisingly, a reentrant metallic behavior is observed with further increasing λ . It is because

the second item of the denominator in eq. (3), originating from the uncompensated carriers, weakens the effect of field on $\rho_{xx}(T, \mu_0 H)$ at low temperature. In the extreme case that the n_e and n_h are severely imbalanced, the upturn behavior even disappears (Fig. 5(d)) since the system will become a (nearly) single-band system where the MR is zero, i.e., the field does not have effect on $\rho_{xx}(T, \mu_0 H)$. Above analysis is still valid when $n > 2$. Noted that recently discovered TaSb₂ [27] exhibits similar behaviors as in LaPn. Thus, it would be interest to examine if our analysis will apply to this system.

Except the electron-hole compensation mechanism, the magnetic field lifting of topologically protected backscattering in topological SMs could also lead to XMR [8]. In these systems, the backscattering is strongly suppressed at zero field, resulting in a transport lifetime τ_{tr} much longer than the quantum lifetime τ_Q . We check this possible mechanism of XMR in LaBi. The $\tau_{tr} = m^* \mu_{e,h}/e$ is $2.59(6) \times 10^{-12}$ s and the ratio τ_{tr}/τ_Q^α (~ 22) is much smaller than those in Dirac SM Cd₃As₂ ($\sim 10^4$) and Weyl SM NbAs ($\sim 10^3$) [7, 8], implying that there may be little topological protection for the α band of LaBi.

In summary, LaBi exhibits the XMR and field-induced resistivity upturn, similar to isostructural LaSb. Based on the two-band model, these behaviors can be well understood and the electron-hole compensation mechanism seems dominant in LaBi. The key conditions leading to the XMR and field-induced properties in SMs are *significantly high $\mu_{e,h}$, extremely small ρ_0 , and rather low $n_{e,h}$ satisfying the compensation condition*. Because theoretical calculation suggests that LaP and LaAs have smaller overlap between electron- and hole-type bands with lower $n_{e,h}$ than LaSb [11], it is worthy inspecting if they will exhibit even larger MR. Systematical studies on LaPn family with simple electron structure will not only deepen our understanding on XMR phenomenon but also shed light on exploring novel XMR materials with prominent properties for potential applications.

This work was supported by the Ministry of Science and Technology of China (973 Project: 2012CB921701), the Fundamental Research Funds for the Central Universities, and the Research Funds of Renmin University of China (14XNLQ03 and 15XNLF06), and the National Nature Science Foundation of China (Grant No. 11574394). Computational resources have been provided by the Physical Laboratory of High Performance Computing at RUC.

† These authors contributed equally to this work.

* hlei@ruc.edu.cn

[1] J. M. Daughton, J. Magn. Magn. Mater. **192**, 334 (1999).
 [2] M. N. Baibich, J. M. Broto, A. Fert, F. Nguyen Van Dau, F. Petroff, P. Etienne, G. Creuzet, A. Friederich, and J.

Chazelas, Phys. Rev. Lett. **61**, 2472 (1988).
 [3] A. P. Ramirez, R. J. Cava, and J. Krajewski, Nature **386**, 156 (1997).
 [4] S. Jin, M. McCormack, T. H. Tiefel, and R. Ramesh, J. Appl. Phys. **76**, 6929 (1994).
 [5] X. C. Huang, L. X. Zhao, Y. J. Long, P. P. Wang, D. Chen, Z. H. Yang, H. Liang, M. Q. Xue, H. M. Weng, Z. Fang, X. Dai, and G. F. Chen, Phys. Rev. X. **5**, 031023 (2015).
 [6] C. Shekhar, A. K. Nayak, Y. Sun, M. Schmidt, M. Nicklas, I. Leermakers, U. Zeitler, Z. K. Liu, Y. L. Chen, W. Schnelle, J. Grin, C. Felser, and B. H. Yan, Nature Phys. **11**, 645 (2015).
 [7] Y. Luo, N. J. Ghimire, M. Wartenbe, H. Choi, M. Neupane, R. D. McDonald, E. D. Bauer, J. Zhu, J. D. Thompson, and F. Ronning, Phys. Rev. B, **92** 205134 (2015).
 [8] T. Liang, Q. Gibson, Mazhar N. Ali, M. H. Liu, R. J. Cava, and N. P. Ong, Nature Mater. **14**, 280 (2015).
 [9] N. A. Mazhar, X. Jun, S. Flynn, T. Jing, Q. D. Gibson, L. M. Schoop, L. Tian, N. Haldolaarachchige, M. Hirschberger, N. P. Ong, and R. J. Cava, Nature. **514**, 205 (2014).
 [10] F. F. Tafti, Q. D. Gibson, S. K. Kushwaha, N. Haldolaarachchige and R. J. Cava, Nature Phys. doi:10.1038/nphys3581 (2015).
 [11] M. G. Zeng, C. Fang, G. Q. Chang, Y. A. Chen, T. Hsieh, A. Bansil, H. Lin, L. Fu, arXiv: 1504.03492 (2015).
 [12] P. E. Blöchl, Phys. Rev. B **50**, 17953 (1994); G. Kresse and D. Joubert, Phys. Rev. B, **59** 1758 (1999).
 [13] G. Kresse and J. Hafner, Phys. Rev. B **47**, 558(R) (1993); G. Kresse and J. Furthmüller, Comp. Mater. Sci. **6**, 15 (1996); Phys. Rev. B **54**, 11169 (1996).
 [14] J. P. Perdew, K. Burke, and M. Ernzerhof, Phys. Rev. Lett. **77**, 3865 (1996).
 [15] N. Marzari and D. Vanderbilt, Phys. Rev. B **56**, 12847 (1997).
 [16] I. Souza, N. Marzari, and D. Vanderbilt, Phys. Rev. B **65**, 035109 (2001).
 [17] A. Kokalj, Comp. Mater. Sci. **28**, 155 (2003).
 [18] Y. L. Wang, L. R. Thoutam, Z. L. Xiao, J. Hu, S. Das, Z. Q. Mao, J. Wei, R. Divan, A. Luican-Mayer, G. W. Crabtree, and W. K. Kwok, Phys. Rev. B **92**, 180402(R) (2015).
 [19] J. M. Ziman, Electrons and Phonons, Classics Series (Oxford University Press, New York, 2001).
 [20] S. Araj and R. V. Colvin, J. Less-Common. Met. **4**, 572 (1962).
 [21] X. Zhang, Z. Xiao, H. C. Lei, Y. Toda, S. Matsuishi, T. Kamiya, S. Ueda, and H. Hosono, Chem. Mater. **26**, 6638 (2014).
 [22] Y. Zhao, H. Liu, J. Yan, W. An, J. Liu, X. Zhang, H. Wang, Y. Liu, H. Jiang, Q. Li, Y. Wang, X.-Z. Li, D. Mandrus, X. C. Xie, M. Pan, and J. Wang, Phys. Rev. B **92**, 041104(R) (2015).
 [23] A. Hasegawa, J. Phys. Soc. Jpn. **54**, 677 (1985).
 [24] D. Shoenberg, Magnetic Oscillations in Metals (Cambridge University Press, Cambridge, England, 1984).
 [25] G. P. Mikitik and Yu. V. Sharlai, Phys. Rev. Lett. **82**, 2147 (1999).
 [26] I. A. Luk'yanchuk, Y. Kopelevich, Phys. Rev. Lett. **93**, 166402 (2004).
 [27] Y. Li, L. Li, J. Wang, T. Wang, X. Xu, C. Xi, C. Cao, and J. Dai, arxiv: 1601.02062 (2016).